DTU

DTU Library

Development of Planar Metal Supported SOFC with Novel Cermet Anode

Blennow Tullmar, Peter; Hjelm, Johan; Klemensø, Trine; Persson, Åsa Helen; Brodersen, Karen; Srivastava, Akhilesh Kumar; Frandsen, Henrik Lund; Lundberg, Mats; Ramousse, Severine; Mogensen, Mogens Bjerg

[Link back to DTU Orbit](#)

Development of Planar Metal Supported SOFC with Novel Cermet Anode

Peter Blennow, Johan Hjelm, Trine Klemensø, Åsa Persson, Karen Brodersen
Akhilesh Kumar Srivastava, Henrik Lund Frandsen, Mats Lundberg
Severine Ramousse, Mogens Mogensen

Fuel Cells and Solid State Chemistry Department, Risø National Laboratory for
Sustainable Energy, Technical University of Denmark, DK-4000 Roskilde, Denmark

Metal-supported solid oxide fuel cells are expected to offer several potential advantages over conventional anode (Ni-YSZ) supported cells, such as increased resistance against mechanical and thermal stresses and a reduction in materials cost. When Ni-YSZ based anodes are used in metal supported SOFC, electrode material from the active anode layer may interdiffuse with the metallic support during sintering. The purpose of this work is to illustrate how the interdiffusion problem can be circumvented by using an alternative anode design based on porous and electronically conducting layers, into which electrocatalytically active materials are infiltrated after sintering. The paper presents the recent results on the electrochemical performance and durability of the novel planar metal-supported SOFC design. The results presented in the paper show that the novel cell and anode design has a promising performance and durability at a broad range of temperatures and is especially suitable for intermediate temperature operation.

Introduction

Solid oxide fuel cells (SOFC) are high temperature electrochemical devices, which convert the energy of a chemical reaction directly into electrical energy. They are normally operated between 600-1000ºC and since high efficiencies can be reached, also for quite small fuel cell units, this technology is attractive for energy conversion systems. However, there are some drawbacks which have caused a slow introduction of SOFCs on the energy market. One of the main problems is the choice of materials in relation to costs. Much of the development of SOFC technology has generally been devoted to reduce the thickness of various cell components. Furthermore, the various components comprising an SOFC are constantly being refined and improved with the overall aim of achieving higher and more stable electrochemical performance with various fuels, while lowering the cost.

The primary challenges to be solved, before fuel cells can achieve a breakthrough on the consumer market, are costs and durability. Investigating different materials and finding new ingenious solutions in design engineering are a few key factors that could make it possible. Low temperature operation (500 – 800ºC) exhibit advantages such as wider choice of component materials (including metals), improved stability, increased material durability and overall device robustness. All these factors aim at crucially lowering the cost of the SOFC device.

Metal supported SOFCs are believed to offer an alternative to conventional electrode- and electrolyte-supported SOFCs. They have many potential advantages such as good thermal conductivity and ductility of the metallic substrate, which may both improve thermal shock resistance, and lower the internal temperature gradients, allowing quicker start-up (1). The metal supported SOFCs also offer low-cost material alternatives compared to traditional all-ceramic-based devices. Furthermore, they have different mechanical behavior, compared to ceramic components, which makes them potential candidates for withstanding the mechanical stresses e.g. generated by the severe vibrations when a stack is incorporated into systems used for transport applications. Despite these potential advantages, processing challenges have been the major issue holding back the development of metal supported SOFCs. One of the most important issues is the densification of the electrolyte layer that normally requires high sintering temperatures (normally > 1200ºC). These high temperatures tend to lead to serious corrosion of the metallic substrate. To solve the problem, different processing routes to fabricate electrodes and dense electrolytes on metallic supports have been employed, such as atmospheric plasma spray processing (APS) (2,3), vacuum plasma spraying (VPS) (4-7), pulsed laser deposition (PLD) (8), electrophoretic deposition (EPD) (9), and high temperature sintering in reducing atmosphere (1,10,11).

Most developers of metal supported SOFCs use anodes that are a ceramic-metallic composite (cermet) of yttria-doped zirconia (YSZ) and nickel. However, at elevated temperatures nickel tends to agglomerate and sinter, resulting in a degradation of the anode performance with time. Furthermore, when Ni-YSZ based anodes are used in metal supported SOFC, electrode material from the active anode layer may interdiffuse with the metallic support during sintering or during high temperature operation. Interdiffusion causes formation of a Ni-Cr-Fe alloy in the anode layer, which is detrimental to cell performance and stability (see e.g. (12) and references therein).

Infiltration of various materials has recently been introduced for use in SOFC electrodes. Infiltration with ceria-based nano-particles, in Ni-YSZ based anodes, has showed sustained sulphur tolerance when operating on humidified H_2 fuel containing 40 ppm H_2S (13). Infiltration of Ni and LSM ($(La,Sr)MnO_3$) in porous YSZ backbone structure for the use as anode and cathode, respectively, in metal supported SOFC has been successfully demonstrated by Tucker et. al. (1). They fabricated a five-layer structure consisting of porous metal-support/porous YSZ interlayer/dense YSZ electrolyte film/porous YSZ interlayer/porous metal current collector. After sealing the cell to a cell housing/gas manifold the porous YSZ interlayers were infiltrated with Ni and LSM catalyst precursor solutions at low temperature prior to cell testing. This fabrication route avoided undesirable decomposition of LSM, Ni coarsening, and interdiffusion between Ni catalyst and FeCr in the support (1). However, the power output of a cell with as-infiltrated Ni anode degraded rapidly during initial operation. This degradation was attributed primarily to coarsening of the fine infiltrated Ni particles (10). It has recently been demonstrated that it is possible to improve the performance for hydrogen oxidation by several orders of magnitude through surfactant-assisted infiltration of a Gd-doped ceria phase (CGO) into an electronically conductive backbone phase consisting of Nb-doped $SrTiO_3$ (STN), which after low-temperature calcination form nano-sized CGO particles on the surface of the electronically conductive backbone structure (14). It was shown that the electrochemical activity was maintained or even improved compared to Ni/YSZ fuel electrodes. The electrocatalytic activity and oxygen

ion transport was believed to be provided by the CGO nano-particle network covering the STN backbone structure whereas the STN backbone structure mainly provided electronic conductivity (14).

Based on the abovementioned challenges with interdiffusion in the Ni-Fe-Cr system and Ni coarsening during operation, this paper presents the development of metal supported cells with a novel design where these problems can be circumvented by using an alternative anode structure. The cell design is based on porous and highly electronically conducting layers into which electrocatalytically active anode materials (CGO and minor amounts of Ni) are infiltrated after sintering. The metal supported cells are developed for operation at lower temperatures in the range 600 – 750ºC (15). Furthermore, the cell design is based on a multilayered structure obtainable by conventional ceramic processing techniques.

Experimental

Sample Fabrication

The metal powder was selected regarding particle size distribution suitable for tape casting. The slurry was based on organic solvent and contained, in addition to the Fe-Cr-powder, binder, plasticizer, and other organic additives necessary for the fabrication process. Some metal-based slurries were also fabricated with 0 – 50 vol.% Y-doped ZrO_2 (YSZ) with respect to metal powder to, after tape-casting, form a so called cermet (ceramic + metal) layer (see Figure 1) of various thicknesses. Similar conventional ceramic processing techniques have been used to fabricate thin electrolyte tapes based on Sc- and Y-doped ZrO_2 (from here on referred to as ScYSZ). After drying, the tapes were laminated together and cut to desired shape. Thereafter, the half cells were heat treated in air for debinding followed by co-sintering in reducing atmosphere (H_2/Ar). After co-sintering, the electrocatalytically active phase (to work as fuel electrode) was infiltrated into the porous structure (see more details below). Similar fabrication route was used to fabricate symmetrical cells of cermet layer/electrolyte (thick)/cermet layer. These symmetrical cells were used to investigate the electrochemical performance of the anode structure in an one atmosphere set-up.

As a final step in the fabrication of a fully functional metal supported SOFC, the cathode layers have been applied by screen printing of $La_{0.58}Sr_{0.4}Co_{0.2}Fe_{0.8}O_{3-\delta}/Ce_{0.9}Gd_{0.1}O_{2-\delta}$ (LSCF/CGO) composite powders.

Catalyst Infiltration

The infiltration of electrocatalysts basically followed the procedure set forth in ref. (14). Table I shows the different compounds that were investigated by infiltration in symmetrical cells.

TABLE I. Prepared infiltration solutions.

Target compound	Abbreviation
CeO_2	CeO_2
$Ce_{0.8}Gd_{0.2}O_{2-\delta}$	CGO20
$Ce_{0.8}Gd_{0.2}O_{2-\delta}$ + 10wt.% Ni	CGO20-Ni

Only the most promising infiltration solution ($Ce_{0.8}Gd_{0.2}O_{1.9}$ (CGO20) + 10 wt.% Ni (with respect to CGO20), CGO20-Ni), based on electrochemical performance as an fuel electrode in symmetrical cell tests (see details below), was further tested for infiltration in half cells with successive application of cathode layers followed by cell testing. The prepared solutions were infiltrated into the open porosities of the co-sintered samples using vacuum-assisted infiltration. After infiltration, the cells were calcined at 350ºC in air for 2 h. The amount of infiltrated material in the porous electrodes was estimated by weighing the cells before and after impregnation and calcination. The approximate weight of the electrolyte was subtracted to get wt.% of infiltrated material in the electrode.

Microstructural Characterization

The microstructure of the samples, both before and after electrochemical characterization, was investigated on fractured cells and on polished cross-sections with a Zeiss Supra 25 scanning electron microscope (SEM) equipped with an x-ray energy dispersive spectrometer (XEDS) and with a Hitachi TM1000 tabletop SEM.

Electrochemical Characterization

Symmetrical Cell Tests. The as-fabricated symmetrical cells (cermet layer / electrolyte (thick) / cermet layer) were cut into smaller pieces (0.6 x 0.6 cm^2) followed by infiltration of materials according to Table I. The electrode polarization resistance (R_P) of the various infiltrated electrodes was then characterized by electrochemical impedance spectroscopy (EIS) in a one-atmosphere set-up. Measurements have been conducted between 600 – 800ºC in various atmospheres with humidified H_2 / N_2 gas mixtures. Before EIS measurements, Pt-paste was applied onto the electrodes to obtain a current collection layer. The impedance spectra of the symmetrical cells were obtained at open circuit potential (OCP) with a Solartron 1260 FRA (frequency range 1 MHz – 50 mHz with 25 mV amplitude). The impedance data were analyzed with ZSimpWin software (EChem Software).

Fuel Cell Tests. The fuel cell performance of a metal supported cell infiltrated with CGO20-Ni have been investigated. The tested cell was a button cell (2 x 2 cm^2 sized pieces) with an active area of 0.5 cm^2 (defined by the screen-printed cathode layer). Pt-mesh and Pt-paste was applied on both electrodes as current collector and a combination of gold rings and glass were used as seals between the cell and the alumina tubes (containing the gas supply and electrical wiring). I-V curves were conducted between 650 – 800 ºC in various atmospheres with water-saturated (at ambient temperature) H_2 / N_2 gas mixtures on the anode side and air or oxygen (O_2) on the cathode side. Galvanostatic durability testing was also carried out in order to assess the effect of the heat treatment on the electrochemical stability of the cell. Testing was carried out at low fuel (H_2 + 3% H_2O) and oxygen utilization (1 – 2%), at 655°C and at a current density of 0.25 A cm^{-2}. The oxidant gas was air. The measurements were conducted with a Solartron 1255B frequency response analyzer in combination with a Solartron 1287A potentiostat. The set-up used for the button cell tests was only used as a screening set-up and was not optimized for detailed electrochemical impedance analysis. Thus, detailed characterization of the polarization resistances was not possible. Measurements are currently being conducted on 5 x 5 cm^2 cells (active area 4 x 4 cm^2) where more thorough analysis is possible. These results will be presented in a forthcoming journal paper.

Results and Discussion

<u>Microstructural Characterization</u>

Micrographs of cross-sections of a half cell and a symmetrical cell after sintering (before infiltration) are shown in Figure 1. The micrographs show that the employed fabrication route gives a metal support layer and a cermet layer that are sufficiently porous for gas transport. The electrolyte layer in Figure 1(A) also seemed to be dense, thereby meeting the requirements of gas tightness. The symmetrical cells had similar cermet layer structure compared with the half cells, achieving comparable microstructures with regards to infiltration and electrochemical characterization.
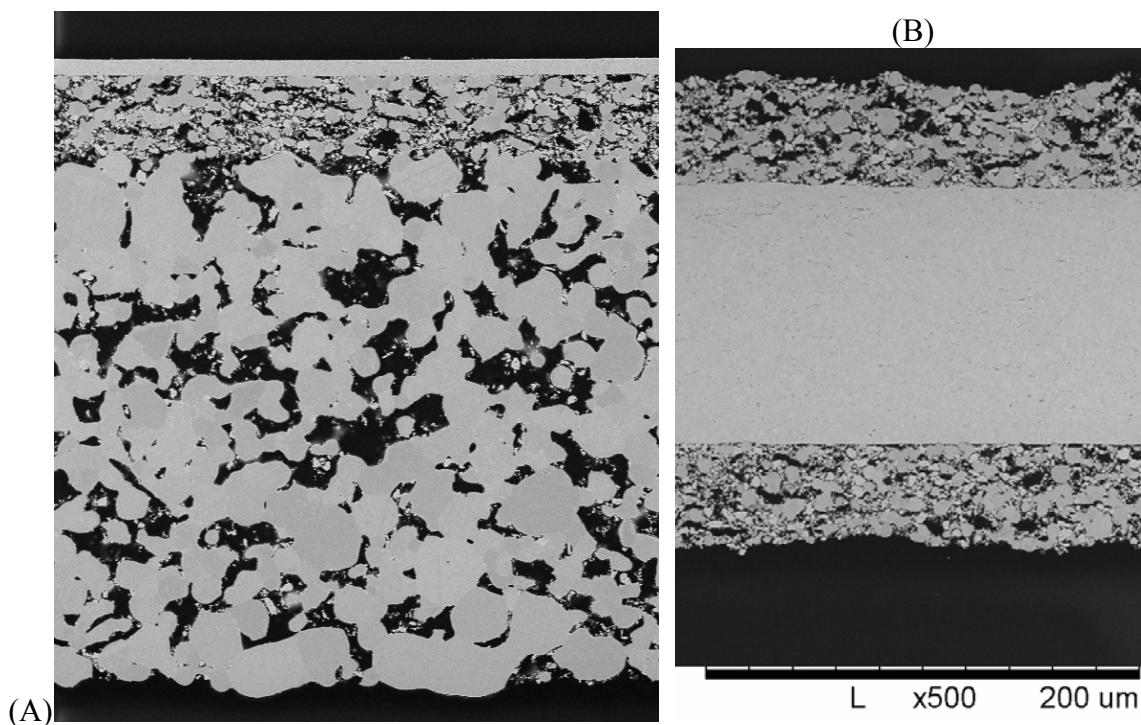

Figure 1. (A) SEM image showing the polished cross-section of the planar metal-supported half cell. The electrolyte is shown in the top, followed by the cermet layer, and the metal support (B) SEM image showing the cross-section of a symmetrical cell of cermet layer/electrolyte/cermet layer before infiltration of electrochemically active material.

Figure 2 displays high magnification SEM images of the microstructure of a fractured symmetrical cell with the cermet layer infiltrated with the CGO20-Ni precursor solution. The nano-sized CGO20-Ni particles completely covered all the cermet particles in the porous microstructure all the way into the electrolyte. The presence of a CGO20 phase was verified with XEDS. Similar microstructures were obtained on the half cells as well but are not shown here.
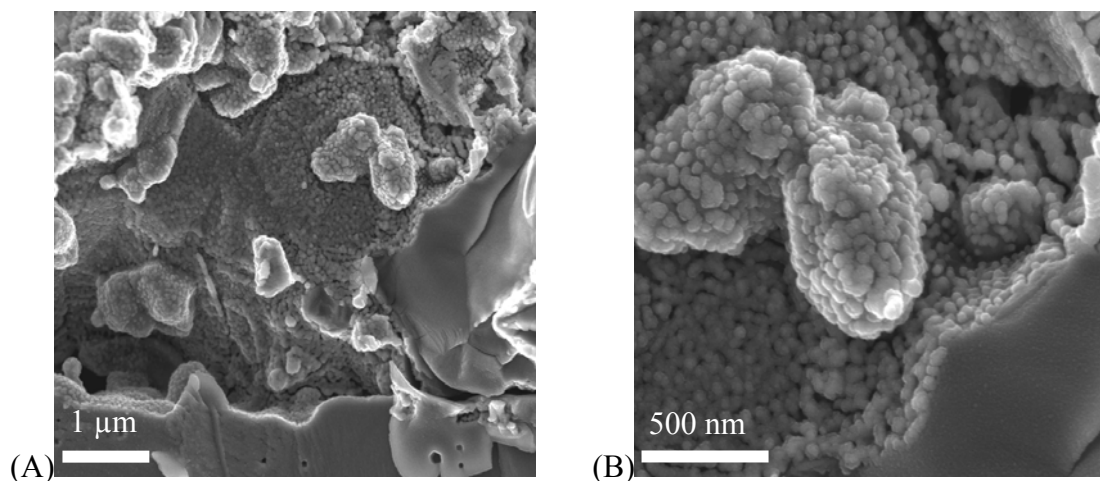
Figure 2. High resolution SEM images at various magnifications showing fractured cross-sectional images of CGO20-Ni infiltrated cermet layers (on symmetrical cells). The CGO20-Ni particles are seen as the thin layer (50 – 100 nm) covering the surfaces of the larger particles in the cermet layer. Part of the electrolyte is seen at the bottom of image (A). The images were obtained after electrochemical testing with a maximum test temperature of 750ºC.

The amount of infiltrated material in the different samples was calculated by weighing the small symmetrical cells and button cells before and after the infiltration steps. The total amount, irrespective of infiltration solution in Table I, was measured to be 10.5 ± 1 wt.% and 2.4 ± 0.2 wt.% for symmetrical cells and button cells, respectively. The samples infiltrated with CGO20-Ni, had 10 wt.% Ni with respect to CGO20. The amount of Ni in the electrodes was thus only approximately 1 wt.% and 0.2 wt.% for the symmetrical cells and button cells, respectively. The amount of infiltrated material between symmetrical cells and button cells should not be directly compared due to the difference in porosity/surface area and weight of the metal support layer and cermet layer. Since the infiltration procedure was identical between the different samples, giving similar microstructures of the infiltrated phase (as identified with SEM), the amount of infiltrated material in the cermet layer in the button cells are believed to be comparable. Since the amount of Ni (NiO) was very small, it was not possible to detect any signal with XEDS during the SEM investigation. However, as the results show, from electrochemical characterization (see details below), there was a dramatic effect with the small additions of Ni to the CGO20 solution. The microstructure of the infiltrated CGO20 phase was similar to the previously reported infiltration of CGO20 in STN backbone (14). Thus, it is believed that the CGO20 grains are only about 5 nm after infiltration and calcination at 350 ºC and reaches a grain size of approximately 40 nm after electrochemical testing at 800ºC, similar to what was reported in ref. (14). The results are consistent with the grain sizes shown in Figure 2. The achieved small CGO20 grain sizes might be explained by a self-limited grain growth mechanism, similar to the results recently reported by Rupp et al. for nano-crystalline ceria ceramics (16). The limited grain growth was only observed for temperatures below 1100ºC and average grain sizes below 140 nm (16). These finding are very interesting for metal supported SOFCs with regards to stability since they are to be used at temperatures < 800ºC where self-limited grain growth of ceria seem to occur.

Electrochemical Characterization

<u>Symmetrical Cell Tests.</u> Examples of impedance spectra, from symmetrical cells infiltrated with CGO20-Ni, obtained between 650 ºC and 750 ºC in H_2 with approximately 3 % H_2O are shown in Figure 3.
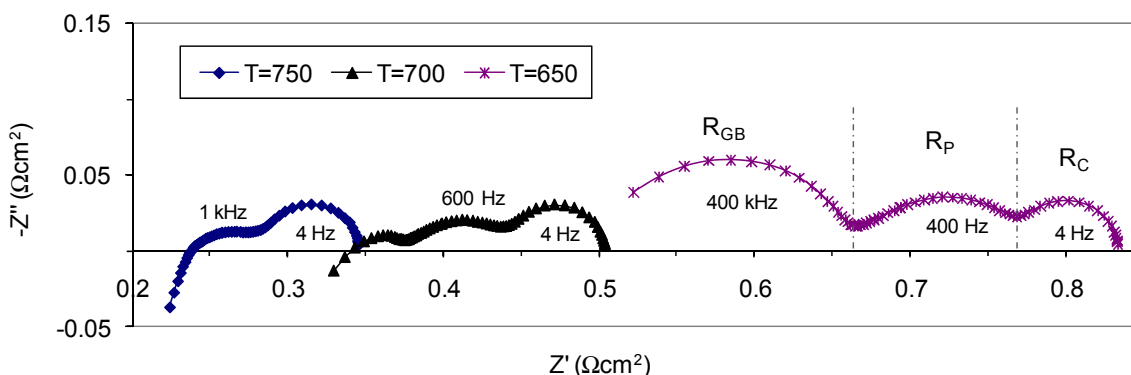

Figure 3. Selected impedance spectra from the symmetrical cells infiltrated with CGO20-Ni at different temperatures in humidified H_2 (approximately 3 % H_2O). All impedance spectra are corrected for the active electrode area (note that R_S must be multiplied by a factor of two for comparison due to the symmetrical cell configuration). R_{GB} = electrolyte grain boundary resistance, R_P = electrode polarization resistance, R_C = concentration polarization (related to test set-up). The frequency numbers indicate the approximate summit frequency of each arc.

From measurements at different temperatures and gas compositions it was found that the impedance data was best fitted to the equivalent circuit $(RQ)_{GB}LR_S(RQ)_P(RC)_C$, following the circuit description codes described elsewhere (17). The inductance, L, is ascribed to the leads and had a typical value of $2 \cdot 10^{-8}$ H for the current measurement system. R_S is ascribed to the series resistance of the symmetric cell, originating mainly from the ionic conductivity of the ScYSZ electrolyte. The magnitude of R_S was as expected for an ScYSZ electrolyte of 120 μm thickness in the investigated temperature range and the results were consistent for all samples. R_{GB} was shown to originate from the contribution from the electrolyte grain boundaries. R_C was in principle temperature independent, however, it was largely affected by changes in pH_2 and/or pH_2O, indicating that this low frequency arc was associated with concentration polarization (related to the test set-up), thus, not related to the electrode polarization resistance (R_P). The polarization resistances (R_P) at 650 ºC for the symmetrical cells with different infiltration solutions are shown in Table II. Only values for 650 ºC are shown due to difficulties in doing the fitting of the impedance data for the other electrodes than those with CGO20-Ni (strong overlap of different semi-circles in the Nyquist plots).

Table II. Polarization resistance (R_P) in Ωcm^2 for different electrode compositions (infiltrated material) measured with symmetrical cells. Each electrode composition was measured on 4 symmetrical cells to check reproducibility.

Electrode composition	R_P @ 650ºC (Ωcm^2)
CeO_2	5.1 ± 0.3
CGO20	1.2 ± 0.2
CGO20-Ni	0.12 ± 0.01

As can be seen in Figure 3 and Table II the R_P for the CGO20-Ni infiltrated electrode was only 0.12 Ωcm^2 and 0.06 Ωcm^2 in humidified hydrogen at 650ºC and 750 ºC, respectively. Furthermore, the apparent activation energy was calculated to 0.62 ± 0.03 eV in the temperature region from 650 – 750ºC, making the electrode especially suitable for intermediate temperature operation. CGO20 is a mixed ionic and electronic conductor (MIEC) and it is therefore believed that the CGO20 is responsible for the electrocatalytic activity with the additional aid of Ni working as a catalyst (18). It is worth noting that the polarization resistance decreased by one order of magnitude with the addition of only 10 wt.% Ni (with respect to CGO20). The cermet layer structure, which is basically only an electronic conductor, is thus believed only to participate in the electrochemistry as a conductor for electrons. The infiltrated phase consisted of nano-sized particles (see Figure 2) and as a result there were active surfaces/facets in large numbers (14), giving rise to the achieved high activity of the CGO20 and CGO20-Ni-infiltrated cermet electrodes.

Fuel Cell Tests. Figure 4 shows polarization and power curves recorded at 655 °C and 749°C. The cell performance was very promising, showing significantly lower or at least comparable area specific resistance (ASR) values than that of many other metal supported SOFCs presented so far in the literature (see e.g ref. (1-11)). The ASR values are calculated as the secant value at 0.6V at the different temperatures and reached 0.26 Ωcm^2 and 0.54 Ωcm^2 at 749 ºC and 655 ºC with hydrogen (with 4% H_2O) as fuel and O_2 as oxidant.
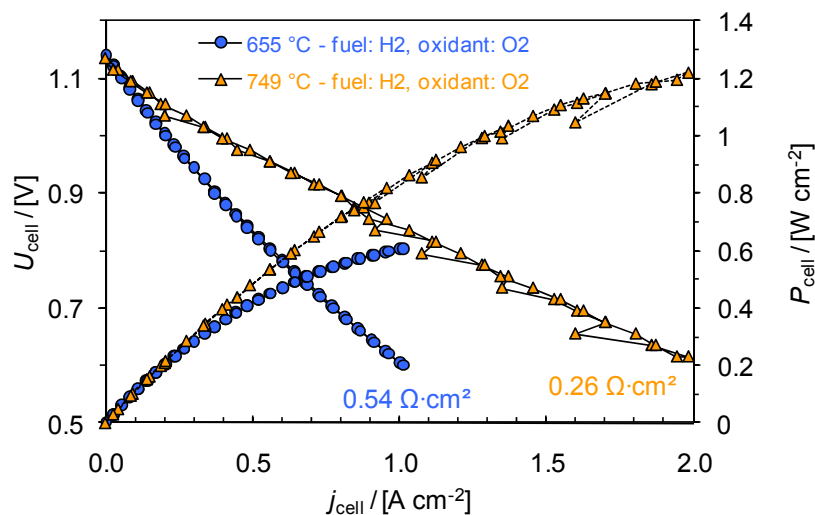

Figure 4. I-V and I-P characteristics of the metal supported button cell at 655ºC and 749ºC. Humidified (approximately 4% H_2O) H_2 as fuel and oxygen (O_2) as oxidant. The inserted numbers are the area specific $ASR_{0.6V,secant}$ values at 0.6V at the respective temperatures.

Figure 5 shows the evolution of the open circuit voltage (OCV) with time at 655ºC and after thermal cyclings up to max 800ºC. The results showed that the button cell had good stability and nice electrolyte gas tightness with no significant increase of ASR with time or by spending up to 20 h at 800ºC. The thermal cyclings (between 650ºC and 800ºC) were done at a rate of 240 ºC/h, a rate which only was limited by the test set-up. Furthermore, the cell voltage reached >1250 mV in dry hydrogen at a flow rate of 12 L h^{-1} cm^{-2} indicating a relatively gas tight cell.
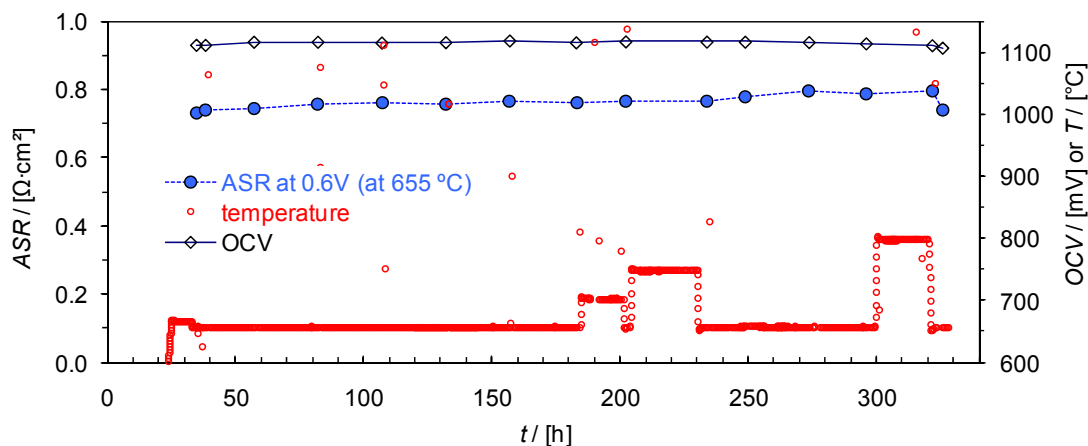
Figure 5. Evolution of the open circuit voltage (OCV) and $ASR_{0.6V,secant}$ at 655 ºC with time and after thermal cyclings up to max 800 ºC. Measurements in humidified (approximately 4% H_2O) H_2 as fuel and air as oxidant.

Figure 6 shows the evolution of the cell voltage with time under a constant current load of 0.25 Acm^{-2} and 655°C for approximately 1000 h. The galvanostatic durability test was conducted after the thermal cyclings shown in Figure 5. The degradation rate observed during testing at 0.25 Acm^{-2} was <5 % / 1000 h based on the change in cell voltage during the testing period. Forthcoming reports will include more detailed analysis of the tested cells with more discussion about the possible degradation mechanisms.
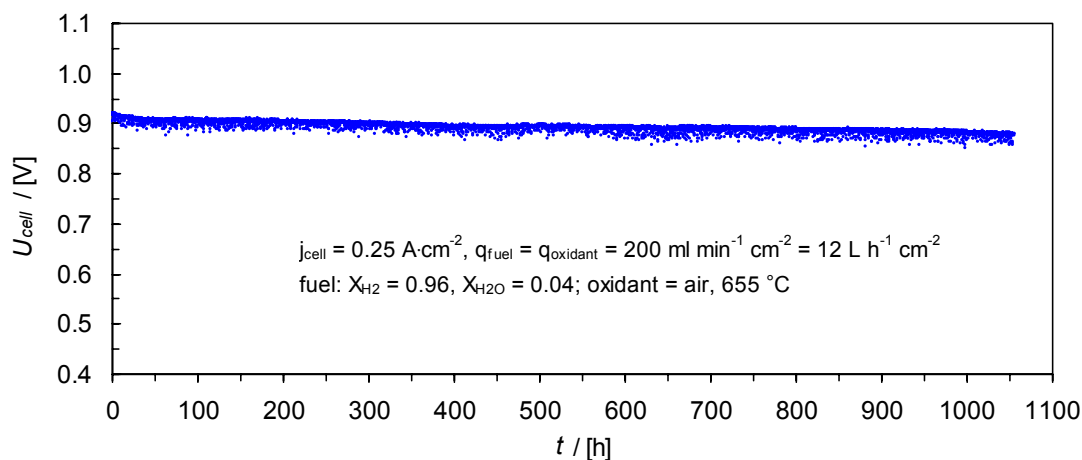

Figure 6. Durability of the metal supported button cell at 655ºC and a current density of 0.25 A cm^{-2}. Humidified (approximately 4% H_2O) H_2 as fuel and air as oxidant.

Conclusions

A novel metal supported SOFC design has been developed, comprising an anode structure, in which nano-sized ceria and nickel particles were formed in a backbone structure of an electronically conductive cermet phase. Nickel was only present in minor amounts to improve the catalytic activity, thereby making the anode structure less sensitive for Ni-agglomeration. The multilayered structure was successfully obtainable by

conventional ceramic processing techniques such as tape-casting, screen printing, and sintering. The results from the symmetrical cells and button cell tests demonstrate fair long-term stability and excellent performance at intermediate temperatures.

Acknowledgments

References

1. M. C. Tucker, G. Y. Lau, C. P. Jacobson, L. C. DeJonghe, S. J. Visco, *J. Power Sources,* **171**, 477 (2007).
2. R. Vassen, D. Hathiramani, J. Mertens, V. A. C. Haanappel, I. C. Vinke, *Surf. Coat. Technol.,* **202**, 499 (2007).
3. R. Vassen, H. Kassner, A. Stuke, F. Hauler, D. Hathiramani, D. Stoever, *Surf. Coat. Technol.,* **202**, 4432 (2008).
4. M. Lang, T. Franco, G. Schiller, N. Wagner, *J. Appl. Electrochem.,* **32**, 871 (2002).
5. M. Lang, P. Szabo, Z. Ilhan, S. Cinque, T. Franco, G. Schiller, *J. Fuel Cell Science and Technology,* **4**, 384 (2007).
6. G. Schiller, T. Franco, M. Lang, P. Metzger, A. Stoermer, *Meet. Abstr. - Electrochem. Soc.,* **501**, 1047 (2006).
7. G. Schiller, A. Ansar, M. Lang, O. Patz, *J. Appl. Electrochem.,* **39**, 293 (2009).
8. S. Hui, D. Yang, Z. Wang, S. Yick, C. Deces-Petit, W. Qu, et al, *J. Power Sources,* **167**, 336 (2007).
9. N. P. Brandon, A. Blake, D. Corcoran, D. Cumming, A. Duckett, K. El-Koury, et al, *J. Fuel Cell Science and Technology,* **1**, 61 (2004).
10. M. C. Tucker, G. Y. Lau, C. P. Jacobson, L. C. DeJonghe, S. J. Visco, *J. Power Sources,* **175**, 447 (2008).
11. Y. B. Matus, L. C. De Jonghe, C. P. Jacobson, S. J. Visco, *Solid State Ionics,* **176**, 443 (2005).
12. M. Brandner, M. Bram, J. Froitzheim, H. P. Buchkremer, D. Stoever, *Solid State Ionics,* **179**, 1501 (2008).
13. H. Kurokawa, G. Y. Lau, C. P. Jacobson, L. C. De Jonghe, S. J. Visco, *J. Mater. Process. Technol.,* **182**, 469 (2007).
14. P. Blennow, K. K. Hansen, L. R. Wallenberg, M. Mogensen, *ECS Trans.,* **13 (26)**, 181 (2008).
15. S. Linderoth, *J. Electroceramics,* **22**, 61 (2009).
16. J. L. M. Rupp, A. Infortuna, L. J. Gauckler, *Acta Mater.,* **54**, 1721 (2006).
17. B. A. Boukamp, *Solid State Ionics,* **169**, 65 (2004).
18. J. Rossmeisl, W. G. Bessler, *Solid State Ionics,* **178**, 1694 (2008).